Thermodynamics investigation of the gas-phase reactions in the chemical vapor deposition of silicon borides with BCl3–SiCl4–H2 precursors

ARTICLE *in* STRUCTURAL CHEMISTRY · OCTOBER 2014

Impact Factor: 1.84 · DOI: 10.1007/s11224-014-0415-5

7 AUTHORS, INCLUDING:

Kehe Su

Northwestern Polytechnical University

41 PUBLICATIONS **209** CITATIONS

SEE PROFILE

Qingfeng Zeng

Northwestern Polytechnical University

99 PUBLICATIONS **835** CITATIONS

SEE PROFILE

Kang Guan

11 PUBLICATIONS **69** CITATIONS

SEE PROFILE

Hui Li

School of Materials Science and Engineering

14 PUBLICATIONS **83** CITATIONS

SEE PROFILE

Struct Chem (2014) 25:1369–1384
DOI 10.1007/s11224-014-0415-5

ORIGINAL RESEARCH

Thermodynamics investigation of the gas-phase reactions in the chemical vapor deposition of silicon borides with BCl_3–$SiCl_4$–H_2 precursors

Haitao Ren · Litong Zhang · Kehe Su · Qingfeng Zeng · Laifei Cheng · Kang Guan · Hui Li

Received: 8 January 2014 / Accepted: 14 February 2014 / Published online: 1 March 2014

Abstract The gas-phase reaction thermodynamics in the chemical vapor deposition (CVD) process of preparing silicon borides with the precursors of BCl_3–$SiCl_4$–H_2 is investigated with a relatively complete set of 220 species, in which the thermochemistry data are calculated with accurate model chemistry at G3(MP2) and G3//B3LYP levels combined with standard statistical thermodynamics. The data include the heat capacities, entropies, enthalpies of formation, and Gibbs free energies of formation. Based on these data, the distribution of the equilibrium concentration of the 220 species is obtained with the principle of chemical equilibrium. $BHCl_2$, $SiHCl_3$, and BH_2Cl are found to be the crucial intermediates. This work provides fundamental data for analyzing the thermochemistry of the CVD process of the BCl_3–$SiCl_4$–H_2 system, which is instructive to optimize the input precursors and temperatures for controlling the composition of the condensed phase B, SiB_6, and SiB_{14}.

Keywords Chemical vapor deposition · Accurate model chemistry · Thermodynamics · Silicon borides

Introduction

Owing to their excellent mechanical, corrosion, and oxidation resistant properties, continuous fiber reinforced silicon carbide matrix composites (CMC-SiC) have been used as advanced thermal protection materials, brake materials in high-temperature structural applications [1–4]. However, a critical drawback of CMC-SiC is the poor oxidation resistance of both the interphase and the fibers [5–7]. Self-healing CMC-SiC were, thus, proposed that contain special elements (e.g., B, BC_x, SiB_x, or Si–B–C) to react with the oxidizing gases. The products were expected viscous glasses which may automatically heal microcracks and pores to slow down the in-depth diffusion of oxidizing gases [8–10]. The B-bearing species can mainly form a glassy phase B_2O_3 at about 500 °C, but it is volatile if the temperature increases, and the self-healing effect is significantly reduced. This limits the working temperatures normally below 1,000 °C [11]. The Si-bearing species can typically form a glassy phase SiO_2 at the temperatures above 1,200 °C and protect CMC-SiC to work at higher temperatures. By involving both Si and B, the self-healing elements will form a mixed glassy phase $SiO_2 \cdot B_2O_3$ that can work at a wider temperature range. Therefore, a broad amount of research has been conducted to prepare silicon borides [12, 13].

Electronic supplementary material The online version of this article (doi:10.1007/s11224-014-0415-5) contains supplementary material, which is available to authorized users.

H. Ren (✉) · L. Zhang · Q. Zeng · L. Cheng · K. Guan
Science and Technology on Thermostructure Composite Materials Laboratory, Northwestern Polytechnical University, Xi'an 710072, Shaanxi, People's Republic of China
e-mail: renht0929@mail.nwpu.edu.cn

K. Su
School of Natural and Applied Sciences, Northwestern Polytechnical University, Xi'an 710072, Shaanxi, People's Republic of China

H. Li
School of Materials Science and Engineering, Chang'an University, Xi'an 710064, Shaanxi, People's Republic of China

H. Li
State Key Laboratory of Solidification Processing, Northwestern Polytechnical University, Xi'an 710072, Shaanxi, People's Republic of China

Chemical vapor deposition (CVD) is one of the most important techniques to prepare silicon borides [14–20]. Since the mechanisms in the CVD process are far from clear, it is desirable to understand the relationship between the deposition condition (e.g., temperature, pressure, or input gas concentrations) and the property of the material [21–23]. For the BCl_3–$SiCl_4$–H_2 system, the associated thermodynamical calculations have not been reported so far. This work will, thus, focus on the reaction thermodynamics for the BCl_3–$SiCl_4$–H_2 CVD system to provide, theoretically, the information about the partial pressure of the possible gaseous species in the system as well as the production of the specific solid phases at different reaction parameters of the CVD process.

Computational methods

There are 220 species involved in this work. The species are chosen for all of the possible ground state molecules and radicals that could be produced by initial dissociation and intermolecular associations in the BCl_3–$SiCl_4$–H_2 system. Because the silicon borides might be important in the nucleation, the clusters up to six heavy atoms are included. The species that have the lowest energy with different spins from the ground state and the energies close to the ground state are also involved. All of the calculations are performed using the GAUSSIAN-09 program [24]. Molecular geometries are completely optimized with density functional theory (DFT) at B3PW91/6-31G(d) level, which has been proven to reproduce the molecular geometries systematically better than a number of other methods [25, 26]. Frequency analyses are performed following each optimization to confirm the stationary structure and to obtain all of the vibrational frequencies. This work employs G3(MP2) [27] and G3//B3LYP [28] methods to evaluate the electronic energies. The heat capacities and entropies at temperatures in 298.15–2,000 K are evaluated with the standard statistical thermodynamics procedures by using the geometries and frequencies (scaled by 0.9573 [30]) calculated with DFT-B3PW91/6-31G(d). The statistical thermodynamics treatments also involve the electronic excitations of low-lying excited states obtained with the time-dependent (TD) B3PW91/6-31G(d) [31–35], and the excitation energies are truncated at 15,000 cm^{-1} or 1.860 eV, which have been reported to be sufficient for electronic contributions to heat capacity and entropy of a molecule at temperature as high as 2,000 K [29]. The enthalpies of formation and Gibbs free energies of formation at 298.15 K are evaluated with statistical thermodynamics, and those for temperatures higher than 298.15 K are calculated classically. Heat capacities as a function of temperature obtained with statistical thermodynamics are fitted into analytical polynomials, and the results are used in developing the enthalpies of formation and Gibbs free energies of formation at any temperature. The enthalpies of formation and Gibbs free energies of formation at 298.15 K are generated with the help of atomization reactions. Chemical potentials are expressed with the ideal gas model. Minimization of the total chemical potential in the system involving all of the 220 species is conducted to evaluate the equilibrium molar values (also concentrations or pressures in a specific volume, equivalently) to obtain the gas-phase diagrams with a code developed in our group [36].

Fig. 1 Numbering, stable structure (symmetry and electronic state) of the 128 new species in the BCl_3–$SiCl_4$–H_2 reaction system obtained with B3PW91/6-31G(d) calculations

Results and discussion

Structure and vibrational frequency

The structure, symmetry, and electronic state of the 128 new species optimized with B3PW91/6-31G(d) in the BCl_3–$SiCl_4$–H_2 reaction system are shown in Fig. 1. Additional 83 species, which are also possible molecules to be involved, taken from Refs. [37, 38] are listed in Table 1. The vibrational frequencies (scaled by the factor 0.9573) and the respective infrared spectra intensities obtained with B3PW91/6-31G(d) are listed in supplement material 1. All of the theoretical frequencies will be used in the statistical thermodynamics calculations.

Electronic excitation energies

It is shown that the electronic excitations are necessary in the statistical evaluations of the thermochemical data. However, the higher (>1.860 eV or 15,000 cm^{-1}) excitations will lead to negligible corrections to the heat capacity or entropy even at higher temperatures up to 2,000 K [29]. So this work only considers the electronic excitation energies less than 1.860 eV. The time-dependent density functional theory (TD-DFT) [31–35] is presently a method which is able to yield the results in a very good agreement with experimental data. All of the 128 new species are calculated with TD-DFT B3PW91/6-31G(d), among which 36 species (listed in supplement 2) were found to have the low-lying excitation energies in the truncation region (1.860 eV). The excitation energies will be used in the statistical thermodynamics calculations for its contribution in the electronic partition functions.

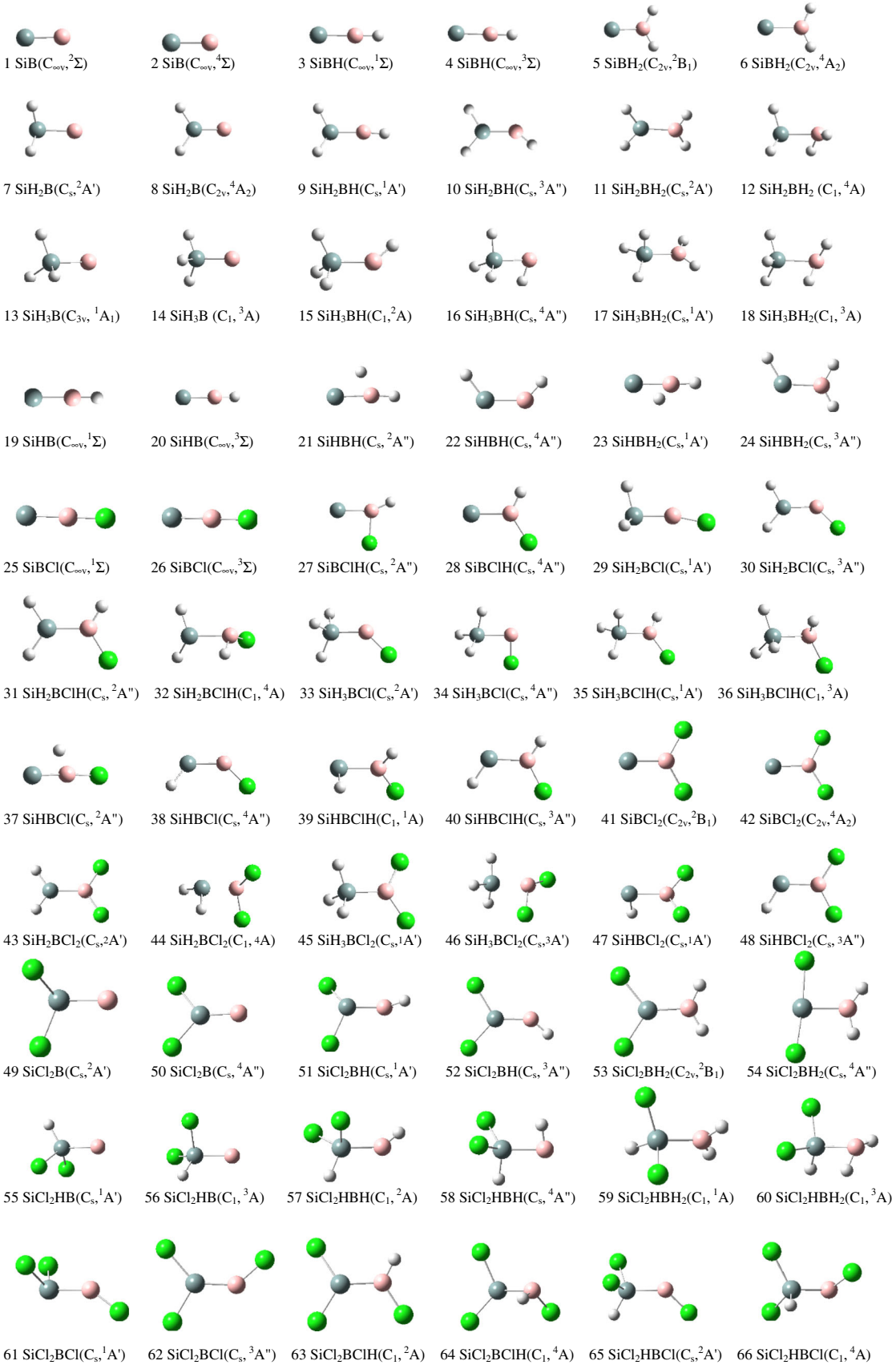
1 SiB($C_{\infty v}$,$^2\Sigma$)
2 SiB($C_{\infty v}$,$^4\Sigma$)
3 SiBH($C_{\infty v}$,$^1\Sigma$)
4 SiBH($C_{\infty v}$,$^3\Sigma$)
5 $SiBH_2$(C_{2v},$^2B_1$)
6 $SiBH_2$(C_{2v},$^4A_2$)
7 SiH_2B(C_s,$^2A'$)
8 SiH_2B(C_{2v},$^4A_2$)
9 SiH_2BH(C_s,$^1A'$)
10 SiH_2BH(C_s,$^3A''$)
11 SiH_2BH_2(C_s,$^2A'$)
12 SiH_2BH_2 (C_1,^4A)
13 SiH_3B(C_{3v}, $^1A_1$)
14 SiH_3B (C_1,^3A)
15 SiH_3BH(C_1,^2A)
16 SiH_3BH(C_s,$^4A''$)
17 SiH_3BH_2(C_s,$^1A'$)
18 SiH_3BH_2(C_1,^3A)
19 SiHB($C_{\infty v}$,$^1\Sigma$)
20 SiHB($C_{\infty v}$,$^3\Sigma$)
21 SiHBH(C_s,$^2A''$)
22 SiHBH(C_s,$^4A''$)
23 $SiHBH_2$(C_s,$^1A'$)
24 $SiHBH_2$(C_s,$^3A''$)
25 SiBCl($C_{\infty v}$,$^1\Sigma$)
26 SiBCl($C_{\infty v}$,$^3\Sigma$)
27 SiBClH(C_s,$^2A''$)
28 SiBClH(C_s,$^4A''$)
29 SiH_2BCl(C_s,$^1A'$)
30 SiH_2BCl(C_s,$^3A''$)
31 SiH_2BClH(C_s,$^2A''$)
32 SiH_2BClH(C_1,^4A)
33 SiH_3BCl(C_s,$^2A'$)
34 SiH_3BCl(C_s,$^4A''$)
35 SiH_3BClH(C_s,$^1A'$)
36 SiH_3BClH(C_1,^3A)
37 SiHBCl(C_s,$^2A''$)
38 SiHBCl(C_s,$^4A''$)
39 SiHBClH(C_1,^1A)
40 SiHBClH(C_s,$^3A''$)
41 $SiBCl_2$(C_{2v},$^2B_1$)
42 $SiBCl_2$(C_{2v},$^4A_2$)
43 SiH_2BCl_2(C_s,$^2A'$)
44 SiH_2BCl_2(C_1,^4A)
45 SiH_3BCl_2(C_s,$^1A'$)
46 SiH_3BCl_2(C_s,$^3A'$)
47 $SiHBCl_2$(C_s,$^1A'$)
48 $SiHBCl_2$(C_s,$^3A''$)
49 $SiCl_2B$(C_s,$^2A'$)
50 $SiCl_2B$(C_s,$^4A''$)
51 $SiCl_2BH$(C_s,$^1A'$)
52 $SiCl_2BH$(C_s,$^3A''$)
53 $SiCl_2BH_2$(C_{2v},$^2B_1$)
54 $SiCl_2BH_2$(C_s,$^4A''$)
55 $SiCl_2HB$(C_s,$^1A'$)
56 $SiCl_2HB$(C_1,^3A)
57 $SiCl_2HBH$(C_1,^2A)
58 $SiCl_2HBH$(C_s,$^4A''$)
59 $SiCl_2HBH_2$(C_1,^1A)
60 $SiCl_2HBH_2$(C_1,^3A)
61 $SiCl_2BCl$(C_s,$^1A'$)
62 $SiCl_2BCl$(C_s,$^3A''$)
63 $SiCl_2BClH$(C_1,^2A)
64 $SiCl_2BClH$(C_1,^4A)
65 $SiCl_2HBCl$(C_s,$^2A'$)
66 $SiCl_2HBCl$(C_1,^4A)

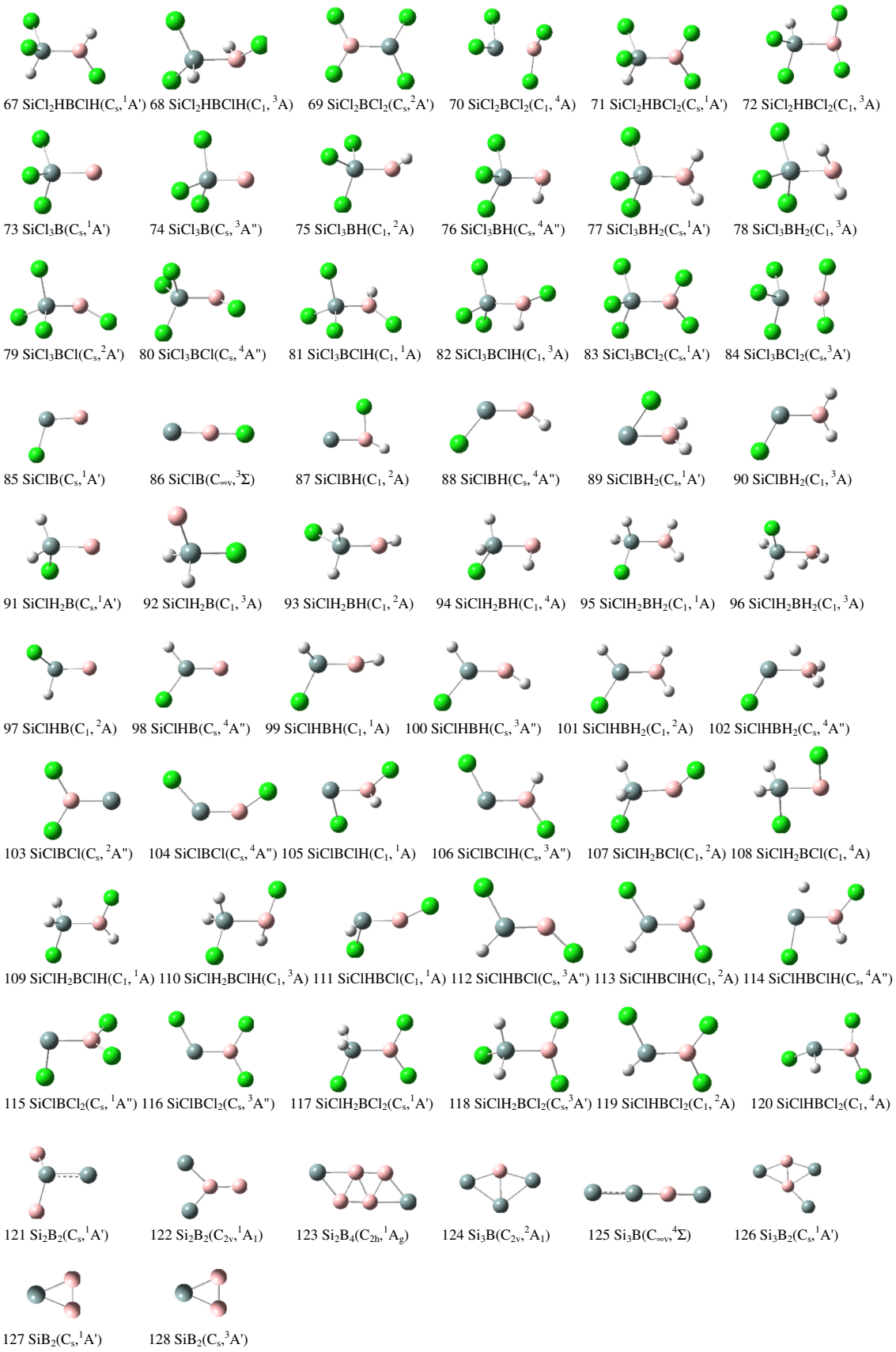

Fig. 1 continued

Table 1 Additional 83 species (symmetry and electronic state) that are possible molecules and atoms in the BCl_3–$SiCl_4$–H_2 reaction system reported previously in Refs. [37, 38]

49 species (symmetry and electronic state) taken from Ref. [37]				
$BH(C_{\infty v},{}^1\Sigma)$	$BH(C_{\infty v},{}^3\Pi)$	$BH_2(C_{2v},{}^2A_1)$	$BH_2(C_{2v},{}^4A_2)$	$BH_3(D_{3h},{}^1A_1')$
$B_2H(C_{\infty v},{}^4\Sigma)$	$HB_2H(D_{\infty h},{}^1\Pi_u)$	$HB_2H(D_{\infty h},{}^3\Sigma_g)$	$B_2H_2(C_{2v},{}^1A_1)$	$B_2H_2(C_{2v},{}^3B_1)$
$HB_2H_2(C_s,{}^2A')$	$B_2H_4(D_{2d},{}^1A_1)$	$B_2H_5(C_{2v},{}^2A_1)$	$B_2H_5(C_s,{}^2A')$	$B_2H_6(D_{2h},{}^1A_g)$
$BCl(C_{\infty v},{}^1\Sigma)$	$BCl(C_{\infty v},{}^3\Pi)$	$BCl_2(C_{2v},{}^2A_1)$	$BCl_3(D_{3h},{}^1A_1')$	$B_2Cl(C_{\infty v},{}^4\Sigma)$
$ClB_2Cl(D_{\infty h},{}^3\Sigma_g)$	$B_2Cl_2(C_{2v},{}^3B_1)$	$ClB_2Cl_2(C_1,{}^2A)$	$B_2Cl_4(D_{2d},{}^1A_1)$	$BHCl(C_s,{}^2A')$
$BH_2Cl(C_{2v},{}^1A_1)$	$BHCl_2(C_{2v},{}^1A_1)$	$HB_2Cl(C_{\infty v},{}^1\Pi)$	$HB_2Cl(C_{\infty v},{}^3\Sigma)$	$B_2HCl(C_s,{}^3A'')$
$H_2B_2Cl(C_s,{}^2A'')$	$H_2B_2Cl\ (C_s,{}^4A'')$	$HB_2ClH(C_s,{}^2A'')$	$HB_2ClH(C_s,{}^4A'')$	$H_2B_2Cl_2(C_{2v},{}^1A_1)$
$HClB_2ClH(C_1,{}^1A)$	$ClB_2ClH(C_s,{}^2A'')$	$ClB_2ClH(C_s,{}^4A'')$	$HB_2Cl_2(C_s,{}^2A'')$	$B_2HCl_2(C_s,{}^4A'')$
$Cl_2B_2HCl\ (C_1,{}^1A)$	$HClB_2H_2(C_1,{}^1A)$	$B_2(D_{\infty h},{}^3\Sigma_g)$	$B_2(D_{\infty h},{}^1\Sigma_g)$	$B_2(D_{\infty h},{}^5\Sigma_u)$
$B_3(D_{3h},{}^2A_1')$	$Cl_2(D_{\infty h},{}^1\Sigma_g)$	$HCl(C_{\infty v},{}^1\Sigma)$	$H_2(D_{\infty h},{}^1\Sigma_g)$	
34 species (symmetry and electronic state) taken from Ref. [38]				
$SiH_3Cl(C_{3v},{}^1A_1)$	$SiCl_3H(C_{3v},{}^1A_1)$	$SiH_2Cl_2(C_{2v},{}^1A_1)$	$HSi_2Cl(C_s,{}^3A'')$	$SiHCl(C_s,{}^1A')$
$SiHCl(C_s,{}^3A'')$	$SiH_2Cl(C_s,{}^2A')$	$SiHCl_2(C_s,{}^2A')$	$SiH(C_{\infty v},{}^2\Pi)$	$SiH_2(C_{2v},{}^1A_1)$
$SiH_2(C_{2v},{}^3B_1)$	$SiH_3(C_{3v},{}^2A_1)$	$SiH_4(T_d,{}^1A_1)$	$Si_2H(C_{2v},{}^2A_1)$	$Si_2H_2(C_{2v},{}^1A_1)$
$Si_2H_3(C_s,{}^2A'')$	$Si_2H_4(C_{2h},{}^1A_g)$	$Si_2H_5(C_s,{}^2A')$	$Si_2H_6(D_{3d},{}^1A_{1g})$	$SiCl(C_{\infty v},{}^2\Pi)$
$SiCl_2(C_{2v},{}^1A_1)$	$SiCl_2(C_{2v},{}^3B_1)$	$SiCl_3(C_{3v},{}^2A_1)$	$SiCl_4(T_d,{}^1A_1)$	$Si_2Cl(C_s,{}^2A'')$
$Si_2Cl_2(C_2,{}^1A)$	$Si_2Cl_3(C_s,{}^2A'')$	$Si_2Cl_4(C_{2h},{}^1A_g)$	$Si_2Cl_5(C_s,{}^2A')$	$Si_2Cl_6(D_{3d},{}^1A_{1g})$
$Si_2(D_{\infty h},{}^3\Sigma_g)$	$Si_2(D_{\infty h},{}^1\Sigma_g)$	$Si_3(C_{2v},{}^1A_1)$	$Si_4(D_{2h},{}^1A_g)$	$Si_2(D_{\infty h},{}^3\Sigma_g)$

Heat capacity and entropy

The structural parameters, vibrational frequencies, and electronic excitation energies obtained in this work are used to calculate the standard molar heat capacity $C^{\theta}_{p,m}$ and entropy S^{θ}_{m} with the standard statistical thermodynamics. The results of 298.15 K are listed in Table 2.

In order to simplify the applications of the high-temperature thermodynamic data, polynomial fitting of the theoretical heat capacities is carried out within 298.15–2,000 K. The data have been fitted into Eq. (1) (consistent with the form of Ref. [39]), and the results are listed in supplement 3.

$$C^{\theta}_{p,m} = a_0 + a_1T + a_2T^2 + a_3T^3 + a_4T^{-2}. \quad (1)$$

As shown in supplement 3, all of the correlation coefficients are larger than 0.999, and most of them are larger than 0.9999. Since the fit is very accurate, this paper will not list the calculated values but the fitting coefficients. The heat capacity as a function of temperature (Eq. (1)) will be used in the high-temperature entropy, enthalpy, and Gibbs free energy evaluations with classical thermodynamics.

Energy

The molecular energies U_0 [sum of electronic energy, spin-orbital coupling ΔE(SO) for atoms, zero point energy E(ZPE), and high-level-correction E(HLC)] obtained with G3(MP2) and G3//B3LYP, the thermal correction to enthalpy (H_{corr}) and to Gibbs free energy (G_{corr}) at 298.15 K are listed in supplement 4. It should be noted that the zero point energies are not included in both of the thermal corrections. Therefore, the standard enthalpy should be U_0 plus H_{corr} and the Gibbs free energy should be U_0 plus G_{corr}.

Standard enthalpies and standard Gibbs free energies of formation

The standard enthalpies of formation $\Delta_f H^{\theta}_m$ (298.15 K) and the standard Gibbs free energies of formation $\Delta_f G^{\theta}_m$ (298.15 K) are calculated with the help of atomization reaction (Eq. (2)). The computational details are shown in Eqs. (3)–(8).

$$aB(g) + bC(g) + cH(g) + dCl(g) \rightarrow B_aC_bH_cCl_d(g), \quad (2)$$

$$\begin{aligned}\Delta_r C^{\theta}_{p,m}(T) = {} & C^{\theta}_{p,m}(B_aC_bH_cCl_d, g, T) - aC^{\theta}_{p,m}(B, g, T) \\ & - bC^{\theta}_{p,m}(C, g, T) - cC^{\theta}_{p,m}(H, g, T) \\ & - dC^{\theta}_{p,m}(Cl, g, T),\end{aligned} \quad (3)$$

$$\begin{aligned}\Delta_r S^{\theta}_{m,298} = {} & S^{\theta}_{m,298}(B_aC_bH_cCl_d,\ g) - aS^{\theta}_{m,298}(B, g) \\ & - bS^{\theta}_{m,298}(C, g) - cS^{\theta}_{m,298}(H, g) \\ & - dS^{\theta}_{m,298}(Cl, g),\end{aligned} \quad (4)$$

$$\Delta_r H^{\theta}_{\mathrm{m},298} = \Delta_f H^{\theta}_{\mathrm{m},298}(\mathrm{B}_a\mathrm{C}_b\mathrm{H}_c\mathrm{Cl}_d,\mathrm{g}) - a\Delta_f H^{\theta}_{\mathrm{m},298}(\mathrm{B},\mathrm{g}) - b\Delta_f H^{\theta}_{\mathrm{m},298}(\mathrm{C},\mathrm{g}) - c\Delta_f H^{\theta}_{\mathrm{m},298}(\mathrm{H},\mathrm{g}) - d\Delta_f H^{\theta}_{\mathrm{m},298}(\mathrm{Cl},\mathrm{g}), \quad (5)$$

$$\Delta_r G^{\theta}_{\mathrm{m},298} = \Delta_f G^{\theta}_{\mathrm{m},298}(\mathrm{B}_a\mathrm{C}_b\mathrm{H}_c\mathrm{Cl}_d,\mathrm{g}) - a\Delta_f G^{\theta}_{\mathrm{m},298}(\mathrm{B},\mathrm{g}) - b\Delta_f G^{\theta}_{\mathrm{m},298}(\mathrm{C},\mathrm{g}) - c\Delta_f G^{\theta}_{\mathrm{m},298}(\mathrm{H},\mathrm{g}) - d\Delta_f G^{\theta}_{\mathrm{m},298}(\mathrm{Cl},\mathrm{g}), \quad (6)$$

$$\Delta_r H^{\theta}_{\mathrm{m}}(T) = \Delta_r H^{\theta}_{\mathrm{m},298} + \int_{298.15\mathrm{K}}^{T} \left(\Delta_r C^{\theta}_{\mathrm{p,m}}(T)\mathrm{d}T\right),$$

$$\Delta_f H^{\theta}_{\mathrm{m}}(\mathrm{B}_a\mathrm{C}_b\mathrm{H}_c\mathrm{Cl}_d,\mathrm{g},T) = \Delta_r H^{\theta}_{\mathrm{m}}(T) + a\Delta_f H^{\theta}_{\mathrm{m}}(\mathrm{B},\mathrm{g},T) + b\Delta_f H^{\theta}_{\mathrm{m}}(\mathrm{C},\mathrm{g},T) + c\Delta_f H^{\theta}_{\mathrm{m}}(\mathrm{H},\mathrm{g},T) + d\Delta_f H^{\theta}_{\mathrm{m}}(\mathrm{Cl},\mathrm{g},T), \quad (7)$$

$$\Delta_r G^{\theta}_{\mathrm{m}}(T) = \Delta_r H^{\theta}_{\mathrm{m}}(T) - T\left[\Delta S^{\theta}_{\mathrm{m},298} + \int_{298.15\mathrm{K}}^{T} \frac{\Delta_r C^{\theta}_{\mathrm{p,m}}(T)}{T}\mathrm{d}T\right],$$

$$\Delta_f G^{\theta}_{\mathrm{m}}(\mathrm{B}_a\mathrm{C}_b\mathrm{H}_c\mathrm{Cl}_d,\mathrm{g},T) = \Delta_r G^{\theta}_{\mathrm{m}}(T) + a\Delta_f G^{\theta}_{\mathrm{m}}(\mathrm{B},\mathrm{g},T) + b\Delta_f G^{\theta}_{\mathrm{m}}(\mathrm{C},\mathrm{g},T) + c\Delta_f G^{\theta}_{\mathrm{m}}(\mathrm{H},\mathrm{g},T) + d\Delta_f G^{\theta}_{\mathrm{m}}(\mathrm{Cl},\mathrm{g},T). \quad (8)$$

The theoretical reaction enthalpy, Gibbs free energy, and entropy at 298.15 K are firstly obtained with the data in Table 2 and supplement 3. The experimental enthalpies of formation $\Delta_f H^{\theta}_{\mathrm{m}}$ (298.15 K) for B, Si, H, and Cl atoms are 565 ± 5, 450 ± 8, 217.999 ± 0.006, and 121.302 ± 0.008 kJ mol^{-1}, respectively. The respective $\Delta_f G^{\theta}_{\mathrm{m}}$ (298.15 K) are 521.0, 405.528, 203.278, and 105.306 kJ mol^{-1}, and the standard entropies S^{θ}_{m} (298.15 K) are 153.436 ± 0.015, 167.871, 114.717, and 165.190 J mol^{-1} K^{-1}. The data of Si, H, and Cl atoms are from Ref. [40], and those of the B are from Ref. [41]. This is because Ref. [41] lists the enthalpy with a smaller uncertainty by 565 ± 5 kJ mol^{-1}, but Ref. [40] lists that with a larger one by 560 ± 12 kJ mol^{-1}. The results at 298.15 K obtained in this work are listed in Table 3.

It is shown in Table 3 that the results obtained from different theoretical methods are basically consistent. Deviations are within 10 kJ mol^{-1} except for thirteen

Table 2 Heat capacity $C^{\theta}_{\mathrm{p.m}}$ and entropy S^{θ}_{m} (298.15 K) calculated with statistical thermodynamics

No.	Species	C_{p} (J mol^{-1} K^{-1})	S (J mol^{-1} K^{-1})
1	SiB($C_{\infty v}$,$^2\Sigma$)	32.40	212.92
2	SiB($C_{\infty v}$,$^4\Sigma$)	32.21	212.65
3	SiBH($C_{\infty v}$,$^1\Sigma$)	41.93	219.42
4	SiBH($C_{\infty v}$,$^3\Sigma$)	42.08	219.47
5	$SiBH_2$(C_{2v},$^2B_1$)	49.25	241.73
6	$SiBH_2$(C_{2v},$^4A_2$)	46.20	237.15
7	SiH_2B(C_s,$^2A'$)	53.96	188.66
8	SiH_2B(C_{2v},$^4A_2$)	47.92	254.19
9	SiH_2BH(C_s,$^1A'$)	59.11	255.43
10	SiH_2BH(C_s,$^3A''$)	58.83	252.49
11	SiH_2BH_2(C_s,$^2A'$)	64.44	259.31
12	SiH_2BH_2(C_1,^4A)	67.94	262.20
13	SiH_3B(C_{3v},$^1A_1$)	58.85	249.55
14	SiH_3B(C_1,^3A)	54.80	251.10
15	SiH_3BH(C_1,^2A)	65.93	266.90
16	SiH_3BH(C_s,$^4A''$)	65.37	260.43
17	SiH_3BH_2(C_s,$^1A'$)	69.69	275.09
18	SiH_3BH_2(C_1,^3A)	74.12	269.46
19	SiHB($C_{\infty v}$,$^1\Sigma$)	41.94	219.42
20	SiHB($C_{\infty v}$,$^3\Sigma$)	42.07	219.45
21	SiHBH(C_s,$^2A''$)	47.55	241.24
22	SiHBH(C_s,$^4A''$)	49.18	243.70
23	$SiHBH_2$(C_s,$^1A'$)	46.94	242.42
24	$SiHBH_2$(C_s,$^3A''$)	55.20	250.42
25	SiBCl($C_{\infty v}$,$^1\Sigma$)	51.90	262.05
26	SiBCl($C_{\infty v}$,$^3\Sigma$)	51.18	256.38
27	SiBClH(C_s,$^2A''$)	54.97	281.99
28	SiBClH(C_s,$^4A''$)	53.99	277.53
29	SiH_2BCl(C_s,$^1A'$)	68.26	290.07
30	SiH_2BCl(C_s,$^3A''$)	68.30	291.27
31	SiH_2BClH(C_s,$^2A''$)	74.31	297.06
32	SiH_2BClH(C_1,^4A)	76.63	298.81
33	SiH_3BCl(C_s,$^2A'$)	72.15	303.94
34	SiH_3BCl(C_s,$^4A''$)	76.03	300.20
35	SiH_3BClH(C_s,$^1A'$)	77.30	309.51
36	SiH_3BClH(C_1,^3A)	82.38	307.38
37	SiHBCl(C_s,$^2A''$)	56.75	276.45
38	SiHBCl(C_s,$^4A''$)	57.74	280.66
39	SiHBClH(C_1,^1A)	66.37	294.82
40	SiHBClH(C_s,$^3A''$)	63.79	286.01
41	$SiBCl_2$(C_{2v},$^2B_1$)	66.57	316.10
42	$SiBCl_2$(C_{2v},$^4A_2$)	65.69	303.26
43	SiH_2BCl_2(C_s,$^2A'$)	87.84	341.06
44	SiH_2BCl_2(C_1,^4A)	89.99	337.23
45	SiH_3BCl_2(C_s,$^1A'$)	89.37	345.19
46	SiH_3BCl_2(C_s,$^3A'$)	94.99	342.64
47	$SiHBCl_2$(C_s,$^1A'$)	77.88	327.38

Table 2 continued

No.	Species	C_p (J mol^{-1} K^{-1})	S (J mol^{-1} K^{-1})
48	$SiHBCl_2(C_s,{}^3A'')$	76.34	317.79
49	$SiCl_2B(C_s,{}^2A')$	72.52	326.36
50	$SiCl_2B(C_s,{}^4A'')$	68.58	313.24
51	$SiCl_2BH(C_s,{}^1A')$	79.33	324.30
52	$SiCl_2BH(C_s,{}^3A'')$	80.17	324.08
53	$SiCl_2BH_2(C_{2v},{}^2B_1)$	85.66	326.62
54	$SiCl_2BH_2(C_s,{}^4A'')$	93.21	344.80
55	$SiCl_2HB(C_s,{}^1A')$	79.00	333.05
56	$SiCl_2HB(C_1,{}^3A)$	76.32	320.37
57	$SiCl_2HBH(C_1,{}^2A)$	88.00	330.63
58	$SiCl_2HBH(C_s,{}^4A'')$	89.92	327.95
59	$SiCl_2HBH_2(C_1,{}^1A)$	91.66	340.65
60	$SiCl_2HBH_2(C_1,{}^3A)$	99.17	339.65
61	$SiCl_2BCl(C_s,{}^1A')$	89.70	362.32
62	$SiCl_2BCl(C_s,{}^3A'')$	88.81	366.29
63	$SiCl_2BClH(C_1,{}^2A)$	94.61	365.97
64	$SiCl_2BClH(C_1,{}^4A)$	100.61	372.35
65	$SiCl_2HBCl(C_s,{}^2A')$	94.78	369.95
66	$SiCl_2HBCl(C_1,{}^4A)$	98.05	366.54
67	$SiCl_2HBClH(C_s,{}^1A')$	99.71	373.75
68	$SiCl_2HBClH(C_1,{}^3A)$	106.03	373.22
69	$SiCl_2BCl_2(C_s,{}^2A')$	106.97	395.47
70	$SiCl_2BCl_2(C_1,{}^4A)$	111.55	403.47
71	$SiCl_2HBCl_2(C_s,{}^1A')$	111.89	409.60
72	$SiCl_2HBCl_2(C_1,{}^3A)$	117.37	408.57
73	$SiCl_3B(C_s,{}^1A')$	92.77	364.32
74	$SiCl_3B(C_s,{}^3A'')$	90.43	350.52
75	$SiCl_3BH(C_1,{}^2A)$	102.59	363.02
76	$SiCl_3BH(C_s,{}^4A'')$	102.84	357.00
77	$SiCl_3BH_2(C_s,{}^1A')$	106.08	371.07
78	$SiCl_3BH_2(C_1,{}^3A)$	112.64	366.97
79	$SiCl_3BCl(C_s,{}^2A')$	109.11	399.68
80	$SiCl_3BCl(C_s,{}^4A'')$	111.65	395.34
81	$SiCl_3BClH(C_1,{}^1A)$	114.03	402.71
82	$SiCl_3BClH(C_1,{}^3A)$	119.61	401.32
83	$SiCl_3BCl_2(C_s,{}^1A')$	126.44	439.56
84	$SiCl_3BCl_2(C_s,{}^3A')$	131.62	437.15
85	$SiClB(C_s,{}^1A')$	49.89	278.21
86	$SiClB(C_{\infty v},{}^3\Sigma)$	51.18	256.40
87	$SiClBH(C_1,{}^2A)$	54.97	281.88
88	$SiClBH(C_s,{}^4A'')$	59.13	281.77
89	$SiClBH_2(C_s,{}^1A')$	63.73	285.53
90	$SiClBH_2(C_1,{}^3A)$	65.45	287.93
91	$SiClH_2B(C_s,{}^1A')$	67.62	298.14
92	$SiClH_2B(C_1,{}^3A)$	66.14	287.91
93	$SiClH_2BH(C_1,{}^2A)$	75.74	295.88
94	$SiClH_2BH(C_1,{}^4A)$	76.47	294.75
95	$SiClH_2BH_2(C_1,{}^1A)$	79.92	304.51

Table 2 continued

No.	Species	C_p (J mol^{-1} K^{-1})	S (J mol^{-1} K^{-1})
96	$SiClH_2BH_2(C_1,{}^3A)$	84.83	304.27
97	$SiClHB(C_1,{}^2A)$	61.42	289.43
98	$SiClHB(C_s,{}^4A'')$	57.24	279.29
99	$SiClHBH(C_1,{}^1A)$	67.63	290.43
100	$SiClHBH(C_s,{}^3A'')$	67.63	289.94
101	$SiClHBH_2(C_1,{}^2A)$	74.26	295.63
102	$SiClHBH_2(C_s,{}^4A'')$	72.80	296.72
103	$SiClBCl(C_s,{}^2A'')$	66.57	321.89
104	$SiClBCl(C_s,{}^4A'')$	67.63	317.86
105	$SiClBClH(C_1,{}^1A)$	75.43	332.75
106	$SiClBClH(C_s,{}^3A'')$	74.44	323.04
107	$SiClH_2BCl(C_1,{}^2A)$	83.78	342.50
108	$SiClH_2BCl(C_1,{}^4A)$	85.68	335.11
109	$SiClH_2BClH(C_1,{}^1A)$	87.87	342.26
110	$SiClH_2BClH(C_1,{}^3A)$	93.11	343.12
111	$SiClHBCl(C_1,{}^1A)$	77.20	326.62
112	$SiClHBCl(C_s,{}^3A'')$	78.49	328.81
113	$SiClHBClH(C_1,{}^2A)$	84.33	343.24
114	$SiClHBClH(C_s,{}^4A'')$	87.48	341.04
115	$SiClBCl_2(C_s,{}^1A'')$	87.25	365.84
116	$SiClBCl_2(C_s,{}^3A'')$	86.41	354.06
117	$SiClH_2BCl_2(C_s,{}^1A')$	99.79	369.64
118	$SiClH_2BCl_2(C_s,{}^3A')$	104.78	377.67
119	$SiClHBCl_2(C_1,{}^2A)$	96.01	363.16
120	$SiClHBCl_2(C_1,{}^4A)$	99.27	372.25
121	$Si_2B_2(C_s,{}^1A')$	72.05	321.31
122	$Si_2B_2(C_{2v},{}^1A_1)$	65.88	311.45
123	$Si_2B_4(C_{2h},{}^1A_g)$	91.37	342.13
124	$Si_3B(C_{2v},{}^2A_1)$	66.95	296.95
125	$Si_3B(C_{\infty v},{}^4\Sigma)$	74.31	321.61
126	$Si_3B_2(C_s,{}^1A')$	81.67	331.17
127	$SiB_2(C_s,{}^1A')$	41.93	331.17
128	$SiB_2(C_s,{}^3A')$	45.85	264.45

species. These are $SiCl_2BCl$(61) by 12.16, $SiCl_2BClH$(64) by 12.69, $SiCl_2HBCl$(66) by 13.81, $SiCl_2HBClH$(68) by 10.04, $SiCl_2BCl_2$(70) by 15.82, $SiCl_3B$(73) by 10.1, $SiCl_3BH$(76) by 11.47, $SiCl_3BH_2$(78) by 10.46, $SiCl_3BCl$(80) by 18.36, $SiCl_3BClH$(82) by 13.64, $SiCl_3BCl_2$(83) by 10.35, $SiCl_3BCl_2$(84) by 21.68, and $SiClHBCl_2$(120) by 13.11 kJ mol^{-1}. The difference is reasonable, since the theoretical levels on electronic energy evaluations and geometry optimizations are different. The results from the higher level G3//B3LYP are expected to be more reliable, but those from G3(MP2) need smaller computational resources and are practical for larger molecules.

Table 3 Standard enthalpies of formation $\Delta_f H_m^\theta$ (298.15 K) and Gibbs free energies of formation $\Delta_f G_m^\theta$ (298.15 K) predicted with G3(MP2) and G3//B3LYP theories

No.	Species	$\Delta_f H_m^\theta$ (298.15 K) (kJ mol^{-1})		$\Delta_f G_m^\theta$ (298.15 K) (kJ mol^{-1})	
		G3(MP2)	G3//B3LYP	G3(MP2)	G3//B3LYP
1	$SiB(C_{\infty v},{}^2\Sigma)$	753.80	754.43	696.81	697.44
2	$SiB(C_{\infty v},{}^4\Sigma)$	686.8	688.95	629.89	632.04
3	$SiBH(C_{\infty v},{}^1\Sigma)$	574.75	573.49	533.57	532.31
4	$SiBH(C_{\infty v},{}^3\Sigma)$	513.97	512.5	472.77	471.31
5	$SiBH_2(C_{2v},{}^2B_1)$	428.83	423.92	398.76	393.85
6	$SiBH_2(C_{2v},{}^4A_2)$	542.82	542.18	514.12	513.48
7	$SiH_2B(C_s,{}^2A')$	600.03	610.11	566.36	576.43
8	$SiH_2B(C_{2v},{}^4A_2)$	663.55	664.46	629.77	630.68
9	$SiH_2BH(C_s,{}^1A')$	397.45	395.49	381.05	379.08
10	$SiH_2BH(C_s,{}^3A'')$	464.19	462.7	448.66	447.17
11	$SiH_2BH_2(C_s,{}^2A')$	268.09	266.0	268.29	266.19
12	$SiH_2BH_2(C_1,{}^4A)$	587.89	588.63	587.22	587.96
13	$SiH_3B(C_{3v},{}^1A_1)$	509.57	509.37	494.92	494.72
14	$SiH_3B(C_1,{}^3A)$	572.14	569.97	557.03	554.86
15	$SiH_3BH(C_1,{}^2A)$	365.12	360.67	363.05	358.6
16	$SiH_3BH(C_s,{}^4A'')$	639.79	638.45	639.65	638.31
17	$SiH_3BH_2(C_s,{}^1A')$	162.02	156.31	175.27	169.56
18	$SiH_3BH_2(C_1,{}^3A)$	428.64	427.21	443.56	442.13
19	$SiHB(C_{\infty v},{}^1\Sigma)$	574.75	573.49	533.57	532.31
20	$SiHB(C_{\infty v},{}^3\Sigma)$	513.98	512.5	472.79	471.31
21	$SiHBH(C_s,{}^2A'')$	428.26	423.35	398.34	393.43
22	$SiHBH(C_s,{}^4A'')$	601.85	602.43	571.2	571.77
23	$SiHBH_2(C_s,{}^1A')$	289.15	288.5	276.63	275.98
24	$SiHBH_2(C_s,{}^3A'')$	405.86	404.19	390.95	389.29
25	$SiBCl(C_{\infty v},{}^1\Sigma)$	389.52	391.61	351.51	353.59
26	$SiBCl(C_{\infty v},{}^3\Sigma)$	331.34	333.24	295.02	296.92
27	$SiBClH(C_s,{}^2A'')$	265.51	265.57	239.31	239.38
28	$SiBClH(C_s,{}^4A'')$	374.99	378.33	350.12	353.46
29	$SiH_2BCl(C_s,{}^1A')$	206.84	209.02	195.99	198.17
30	$SiH_2BCl(C_s,{}^3A'')$	293.93	297.13	282.72	285.92
31	$SiH_2BClH(C_s,{}^2A'')$	101.16	102.03	105.97	106.85
32	$SiH_2BClH(C_1,{}^4A)$	429.84	433.77	434.13	438.06
33	$SiH_3BCl(C_s,{}^2A')$	175.86	175.13	178.63	177.9
34	$SiH_3BCl(C_s,{}^4A'')$	2,070.9	2,071.1	2,092.5	2,092.7
35	$SiH_3BClH(C_s,{}^1A')$	−22.185	−24.553	−3.322	−5.6902
36	$SiH_3BClH(C_1,{}^3A)$	1,800.8	1,799.7	1,838.1	1,836.9
37	$SiHBCl(C_s,{}^2A'')$	265.96	263.33	241.42	238.78
38	$SiHBCl(C_s,{}^4A'')$	429.25	433.43	403.45	407.62
39	$SiHBClH(C_1,{}^1A)$	189.97	188.58	177.7	176.3
40	$SiHBClH(C_s,{}^3A'')$	238.13	240.26	228.49	230.62
41	$SiBCl_2(C_{2v},{}^2B_1)$	93.481	96.038	72.988	75.545
42	$SiBCl_2(C_{2v},{}^4A_2)$	217.64	225.19	200.98	208.53
43	$SiH_2BCl_2(C_s,{}^2A')$	−64.231	−63.215	−56.664	−55.648
44	$SiH_2BCl_2(C_1,{}^4A)$	305.53	307.17	314.23	315.88
45	$SiH_3BCl_2(C_s,{}^1A')$	−201.01	−200.43	−176.91	−176.33
46	$SiH_3BCl_2(C_s,{}^3A')$	137.8	142.38	162.65	167.23
47	$SiHBCl_2(C_s,{}^1A')$	12.092	14.055	5.984	7.9479
48	$SiHBCl_2(C_s,{}^3A'')$	70.666	76.206	67.423	72.963

Table 3 continued

No.	Species	$\Delta_f H_m^\theta$ (298.15 K) (kJ mol^{-1})		$\Delta_f G_m^\theta$ (298.15 K) (kJ mol^{-1})	
		G3(MP2)	G3//B3LYP	G3(MP2)	G3//B3LYP
49	$SiCl_2B(C_s,{}^2A')$	274.04	281.11	250.48	257.55
50	$SiCl_2B(C_s,{}^4A'')$	309.29	316.89	289.65	297.25
51	$SiCl_2BH(C_s,{}^1A')$	77.312	83.663	72.123	78.474
52	$SiCl_2BH(C_s,{}^3A'')$	113.06	118.38	107.93	113.26
53	$SiCl_2BH_2(C_{2v},{}^2B_1)$	−79.012	−76.059	−67.138	−64.184
54	$SiCl_2BH_2(C_s,{}^4A'')$	307.2	314.54	313.65	320.98
55	$SiCl_2HB(C_s,{}^1A')$	162.03	169.87	154.24	162.07
56	$SiCl_2HB(C_1,{}^3A)$	222.48	227.04	218.47	223.02
57	$SiCl_2HBH(C_1,{}^2A)$	13.285	15.992	23.959	26.666
58	$SiCl_2HBH(C_s,{}^4A'')$	283.82	292.65	295.3	304.13
59	$SiCl_2HBH_2(C_1,{}^1A)$	−191.02	−190.08	−165.57	−164.63
60	$SiCl_2HBH_2(C_1,{}^3A)$	74.959	80.982	100.7	106.72
61	$SiCl_2BCl(C_s,{}^1A')$	−113.83	−101.67	−114.48	−102.32
62	$SiCl_2BCl(C_s,{}^3A'')$	−45.417	−36.803	−47.249	−38.635
63	$SiCl_2BClH(C_1,{}^2A)$	−233.21	−227.63	−217.18	−211.61
64	$SiCl_2BClH(C_1,{}^4A)$	105.01	117.7	119.12	131.81
65	$SiCl_2HBCl(C_s,{}^2A')$	−172.91	−167.28	−158.08	−152.45
66	$SiCl_2HBCl(C_1,{}^4A)$	184.86	198.67	200.7	214.51
67	$SiCl_2HBClH(C_s,{}^1A')$	−374.79	−370.71	−343.33	−339.26
68	$SiCl_2HBClH(C_1,{}^3A)$	−81.699	−71.654	−50.093	−40.048
69	$SiCl_2BCl_2(C_s,{}^2A')$	−405.95	−396.38	−382.85	−373.29
70	$SiCl_2BCl_2(C_1,{}^4A)$	−40.267	−24.446	−19.564	−3.7425
71	$SiCl_2HBCl_2(C_s,{}^1A')$	−553.01	−545.96	−516.36	−509.32
72	$SiCl_2HBCl_2(C_1,{}^3A)$	−1,731.6	−1,728.1	−1,712.4	−1,708.9
73	$SiCl_3B(C_s,{}^1A')$	1,506	1,516.1	1,522.5	1,532.6
74	$SiCl_3B(C_s,{}^3A'')$	43.348	51.569	46.216	54.436
75	$SiCl_3BH(C_1,{}^2A)$	−167.48	−161.55	−150.59	−144.66
76	$SiCl_3BH(C_s,{}^4A'')$	110.08	121.55	128.76	140.24
77	$SiCl_3BH_2(C_s,{}^1A')$	−374.89	−370.45	−342.64	−338.2
78	$SiCl_3BH_2(C_1,{}^3A)$	−99.978	−89.521	−66.513	−56.055
79	$SiCl_3BCl(C_s,{}^2A')$	−357.21	−347.61	−335.37	−325.77
80	$SiCl_3BCl(C_s,{}^4A'')$	11.526	29.881	34.655	53.01
81	$SiCl_3BClH(C_1,{}^1A)$	−559.27	−551.56	−520.58	−512.87
82	$SiCl_3BClH(C_1,{}^3A)$	−257.66	−244.02	−218.56	−204.92
83	$SiCl_3BCl_2(C_s,{}^1A')$	−736.89	−726.54	−693.31	−682.96
84	$SiCl_3BCl_2(C_s,{}^3A')$	−378.33	−356.65	−334.04	−312.36
85	$SiClB(C_s,{}^1A')$	528.69	536.15	485.87	493.33
86	$SiClB(C_{\infty v},{}^3\Sigma)$	331.34	333.24	295.02	296.91
87	$SiClBH(C_1,{}^2A)$	266.48	263.1	240.32	236.94
88	$SiClBH(C_s,{}^4A'')$	408.08	412.49	381.94	386.35
89	$SiClBH_2(C_s,{}^1A')$	160.02	162.1	150.52	152.6
90	$SiClBH_2(C_1,{}^3A)$	220.05	221.75	209.83	211.53
91	$SiClH_2B(C_s,{}^1A')$	342.33	345.95	329.07	332.69
92	$SiClH_2B(C_1,{}^3A)$	396.59	397.24	386.38	387.03
93	$SiClH_2BH(C_1,{}^2A)$	190.01	188.84	195.18	194
94	$SiClH_2BH(C_1,{}^4A)$	461.13	464.77	466.63	470.27
95	$SiClH_2BH_2(C_1,{}^1A)$	−10.41	−13.137	9.9394	7.2115
96	$SiClH_2BH_2(C_1,{}^3A)$	252.58	253.88	272.99	274.3

Table 3 continued

No.	Species	$\Delta_f H_m^\theta$ (298.15 K) (kJ mol^{-1})		$\Delta_f G_m^\theta$ (298.15 K) (kJ mol^{-1})	
		G3(MP2)	G3//B3LYP	G3(MP2)	G3//B3LYP
97	$SiClHB(C_1,{}^2A)$	451.4	453.99	422.99	425.57
98	$SiClHB(C_s,{}^4A'')$	482.26	486.38	456.87	460.99
99	$SiClHBH(C_1,{}^1A)$	243.21	245.46	232.25	234.5
100	$SiClHBH(C_s,{}^3A'')$	283.12	284.96	272.31	274.14
101	$SiClHBH_2(C_1,{}^2A)$	95.014	95.541	100.26	100.78
102	$SiClHBH_2(C_s,{}^4A'')$	396.69	399.93	401.61	404.84
103	$SiClBCl(C_s,{}^2A'')$	93.484	96.022	71.263	73.802
104	$SiClBCl(C_s,{}^4A'')$	245.38	253.32	224.36	232.3
105	$SiClBClH(C_1,{}^1A)$	−7.2584	−3.4252	−14.962	−11.129
106	$SiClBClH(C_s,{}^3A'')$	59.755	65.166	54.947	60.358
107	$SiClH_2BCl(C_1,{}^2A)$	7.1252	8.9263	14.266	16.067
108	$SiClH_2BCl(C_1,{}^4A)$	370.26	374.06	381.75	383.40
109	$SiClH_2BClH(C_1,{}^1A)$	−193.66	−192.96	−168.68	−167.98
110	$SiClH_2BClH(C_1,{}^3A)$	99.321	103.9	124.03	128.61
111	$SiClHBCl(C_1,{}^1A)$	54.341	61.144	48.465	55.267
112	$SiClHBCl(C_s,{}^3A'')$	127.78	133.14	121.25	126.61
113	$SiClHBClH(C_1,{}^2A)$	−63.275	−62.198	−56.355	−55.278
114	$SiClHBClH(C_s,{}^4A'')$	267.1	274.06	274.67	281.64
115	$SiClBCl_2(C_s,{}^1A'')$	−186.97	−179.89	−188.66	−181.59
116	$SiClBCl_2(C_s,{}^3A'')$	−103.84	−94.8	−102.02	−92.983
117	$SiClH_2BCl_2(C_s,{}^1A')$	−373.47	−369.66	−340.79	−336.98
118	$SiClH_2BCl_2(C_s,{}^3A')$	−5.215	−4.0949	24.614	26.335
119	$SiClHBCl_2(C_1,{}^2A)$	−231.42	−226.38	−214.56	−209.52
120	$SiClHBCl_2(C_1,{}^4A)$	149.97	163.08	164.12	177.22
121	$Si_2B_2(C_s,{}^1A')$	766.18	770.55	683.33	687.7
122	$Si_2B_2(C_{2v},{}^1A_1)$	920.97	917.55	841.06	837.64
123	$Si_2B_4(C_{2h},{}^1A_g)$	968.67	959.92	881.07	872.33
124	$Si_3B(C_{2v},{}^2A_1)$	725.62	727.33	653.47	656.76
125	$Si_3B(C_{\infty v},{}^4\Sigma)$	1,053.2	1,058.7	975.29	980.73
126	$Si_3B_2(C_s,{}^1A')$	801.95	798.38	721.91	718.34
127	$SiB_2(C_s,{}^1A')$	745.9	749.35	678.24	681.69
128	$SiB_2(C_s,{}^3A')$	842.62	839.75	770.99	768.12

Gas-phase equilibrium diagrams

Gas-phase equilibrium concentration distribution of the 220 species involved in the BCl_3–$SiCl_4$–H_2 system as a function of temperature can be obtained according to the principle of chemical equilibrium by minimizing the total Gibbs free energy of the system, as shown in Eq. (9):

$$\min G = \min\left\{\sum_{i=1}^{s} n_i^{\mathrm{cond}} \Delta G_{\mathrm{m},i}^{\theta}(\mathrm{cond.}) + \sum_{i=s+1}^{N} n_i\left[\Delta G_{\mathrm{m},i}^{\theta}(\mathrm{gas}) + RT\ln p + RT\ln\frac{n_i}{\sum_{j=s+1}^{N} n_j}\right]\right\}, \tag{9}$$

where s is the total number of the condensed phase species, N the total number of species in the system, p the total pressure of the system, n_i the number of moles of the ith gaseous species, and n_i^{cond} the number of moles of the ith condensed phase species both satisfy:

$$\sum_{i=1}^{N} a_{ij} n_i = B_j \ (j = 1, 2, \ldots, M),$$

where a_{ij} is the atomicity of element j in species i, B_j the total atomicity of element j, and M the total number of different elements.

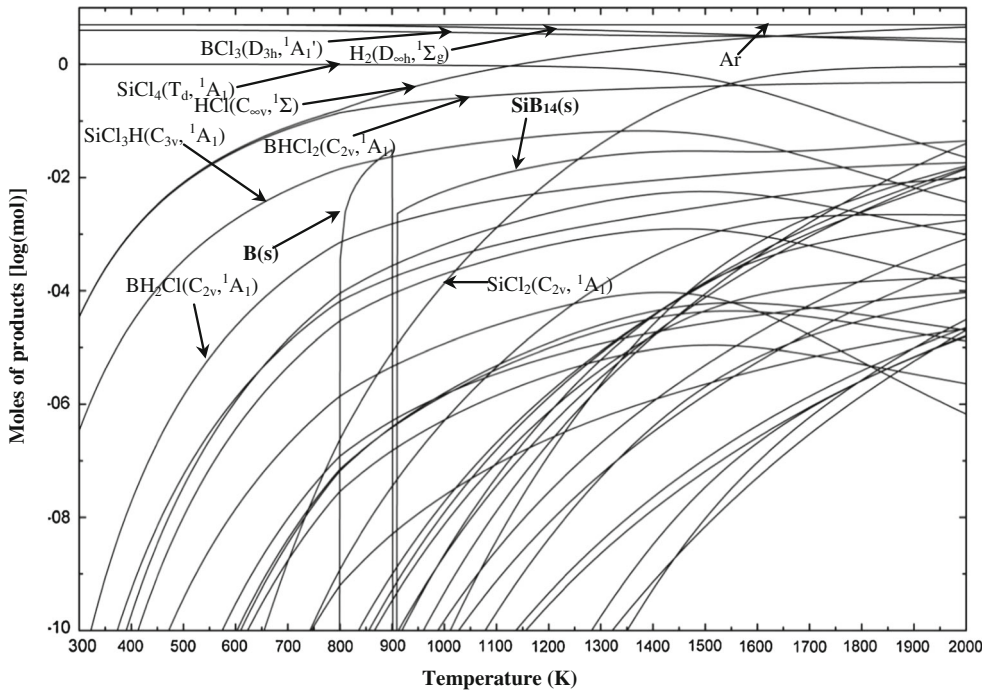

Fig. 2 Equilibrium concentration distribution of the 220 species involved in the process of CVD preparation of silicon borides with BCl_3:$SiCl_4$:H_2:Ar = 4:1:5:5 precurses at 1 atm and in 300–2,000 K (the species having a maximum concentration larger than 10^{-6} mol are shown in this figure)

In Eq. (9), the standard molar Gibbs free energy, either for condensed phase $\Delta G_{\mathrm{m}}^{\theta}$(cond.) or for gaseous species $\Delta G_{\mathrm{m}}^{\theta}$(gas), at any temperature T is defined as the Gibbs energy equation:

$$\Delta G_{\mathrm{m}}^{\theta}(T) = \Delta H_{\mathrm{m}}^{\theta}(T) - T \cdot \Delta S_{\mathrm{m}}^{\theta}(T).$$

In which

$$\Delta H_{\mathrm{m}}^{\theta}(T) = \Delta_{\mathrm{f}} H_{\mathrm{m}}^{\theta}(298.15\ \mathrm{K}) + \int_{298.15}^{T} C_{\mathrm{p,m}}\mathrm{d}T,$$

$$\Delta S_{\mathrm{m}}^{\theta}(T) = S_{\mathrm{m}}^{\theta}(298.15\ \mathrm{K}) + \int_{298.15}^{T} \frac{C_{\mathrm{p,m}}}{T}\mathrm{d}T,$$

where the heat capacity in the integrals is for the species itself rather than the reaction of formation (and therefore, the final result is not exactly the data of formation at temperatures other than 298.15 K).

By using the predicted enthalpies of formation at 298.15 K for all the 211 gas-phase species (Table 3 and Refs. [37, 38]), combined with the fitted heat capacities (supplement 3 and Refs. [37, 38]) and the data of the Si, B, H, and Cl atoms, those of the condensed phases Si, B, SiB_3, SiB_6 and SiB_{14} from Refs. [40, 41], the equilibrium concentration distribution for all of the species is calculated according to Eq. (2) with the code [36] developed in our group (the correctness has been confirmed compared with the examples of the FactSage [42]). The results are shown in Fig. 2, where the total pressure is 1 atm, and the molar ratio of the input gases BCl_3:$SiCl_4$:H_2:Ar is 4:1:5:5.

The curves plotted in Fig. 2 are the overview of the equilibrium concentration distribution for the species having the maximum concentration (denoted by moles in a specific volume) higher than 1×10^{-6} mol in our temperature region 300–2,000 K. Figure 3a shows the distribution of the reactants. Figure 3b shows the distribution of the species having the maximum concentration above 10^{-3} mol, and Fig. 3c shows those having the concentration between 10^{-3} and 10^{-5} mol. Figure 3d shows the distribution of the species having the concentration between 10^{-6} and 10^{-7} mol.

Figure 3a shows that each of the concentration of the reactants H_2, BCl_3, and $SiCl_4$ decreases at the temperatures higher than 500 K and, consequently, Fig. 3b shows that the amount of the products HCl, $BHCl_2$, $SiHCl_3$, and BH_2Cl increases. This implies that the consumption of BCl_3 is directly related to the production of HCl, $BHCl_2$, and BH_2Cl according to the reaction

$$BCl_3 + H_2 \rightarrow BHCl_2 + HCl.$$

This result agrees with that of Ref. [21]. The increase of $SiHCl_3$ and BH_2Cl can be explained by the reactions of

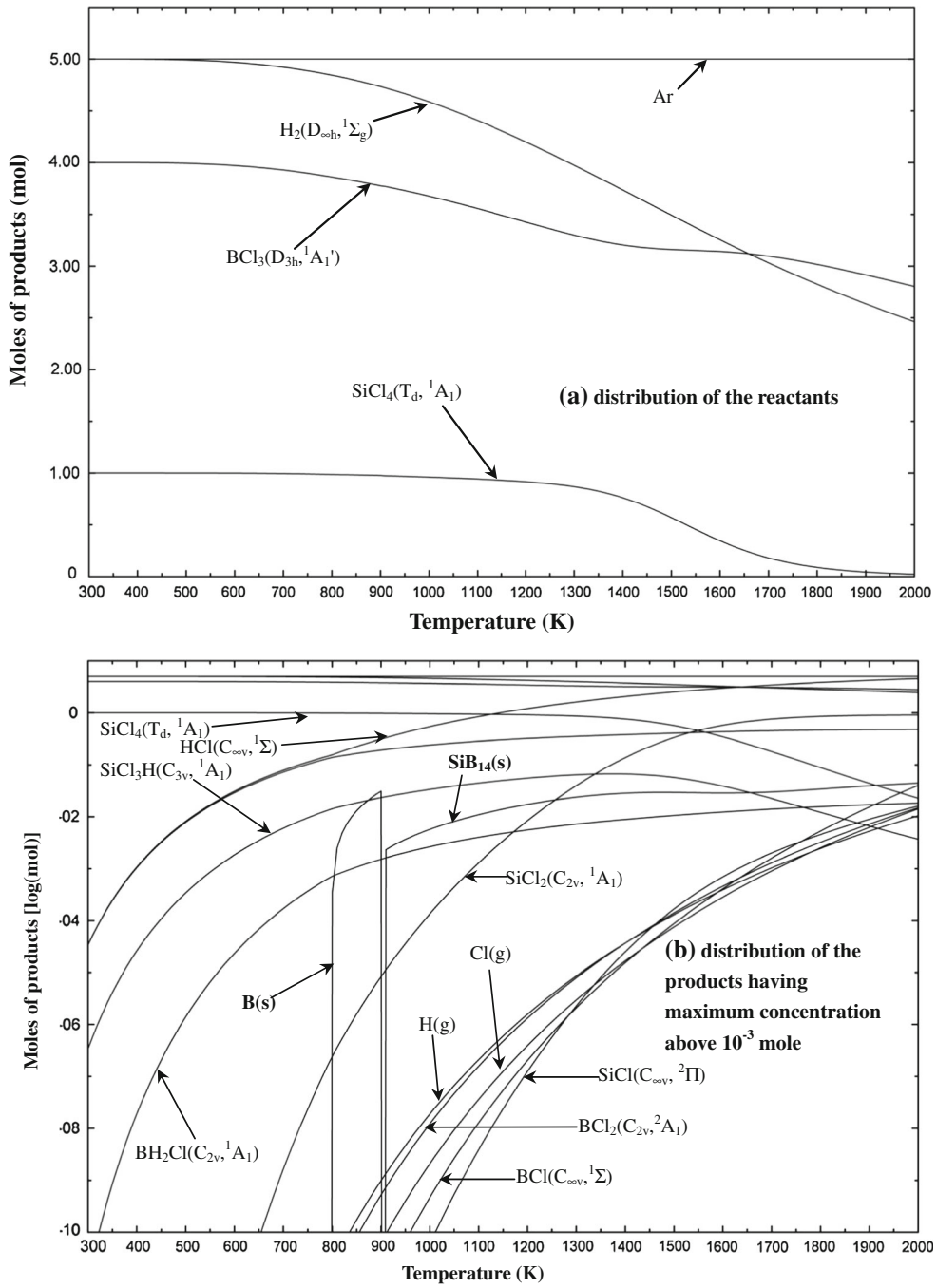

Fig. 3 Equilibrium concentration distribution

$$BCl_3 + H_2 \rightarrow BH_2Cl + HCl$$
$$SiCl_4 + H_2 \rightarrow SiHCl_3 + HCl.$$

Figure 3b also shows that $SiCl_2$ is generated at about 660 K, and its concentration increases rapidly with temperature. Figure 3c indicates that the production of $SiCl_3BCl_2$, B_2Cl_4, and SiH_2Cl_2 increases rapidly with temperature. The associated reactions should be

$$SiCl_4 + BCl_3 + H_2 \rightarrow SiCl_3BCl_2 + HCl$$
$$2BCl_3 + H_2 \rightarrow B_2Cl_4 + HCl$$
$$SiCl_4 + H_2 \rightarrow SiH_2Cl_2 + HCl$$
$$SiCl_4 + H_2 \rightarrow SiCl_2 + HCl.$$

Other species that might also be important are H, BCl_2, Cl, BCl, Si_2Cl_6, $SiCl_3$, etc. as shown in Figs. 3b–d. The associated reactions may be

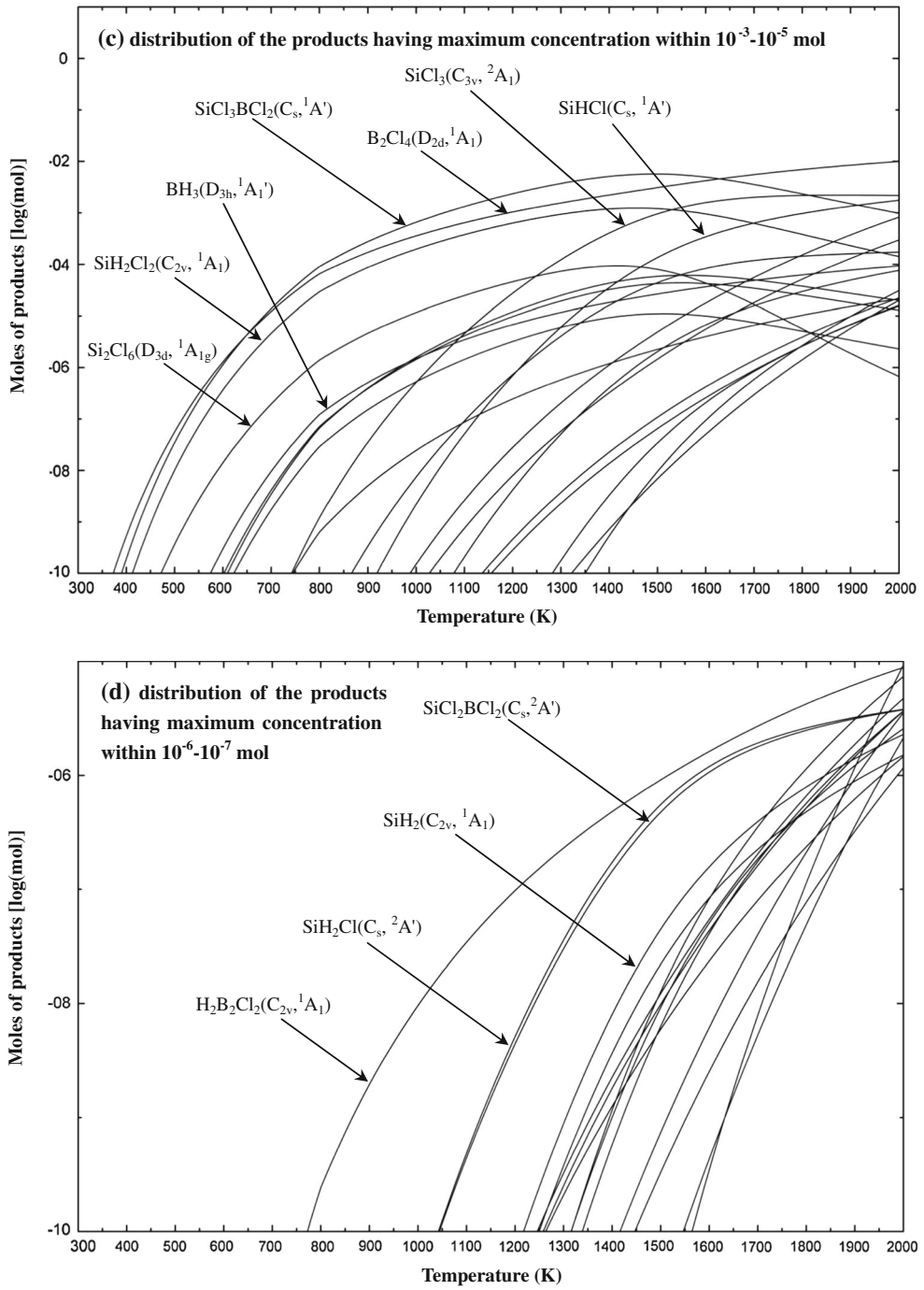

Fig. 3 continued

$$H_2 \rightarrow H$$
$$BCl_3 \rightarrow BCl_2 + Cl$$
$$BCl_2 \rightarrow BCl + Cl$$
$$2SiCl_4 \rightarrow Si_2Cl_6 + Cl$$
$$SiCl_4 \rightarrow SiCl_3 + Cl.$$

For the condensed phases, both of Figs. 2 and 3b show that the pure boron can only be produced within 800–900 K with a high yield. For temperatures higher than 910 K, the boron rich SiB_{14} phase is produced instead of the pure boron.

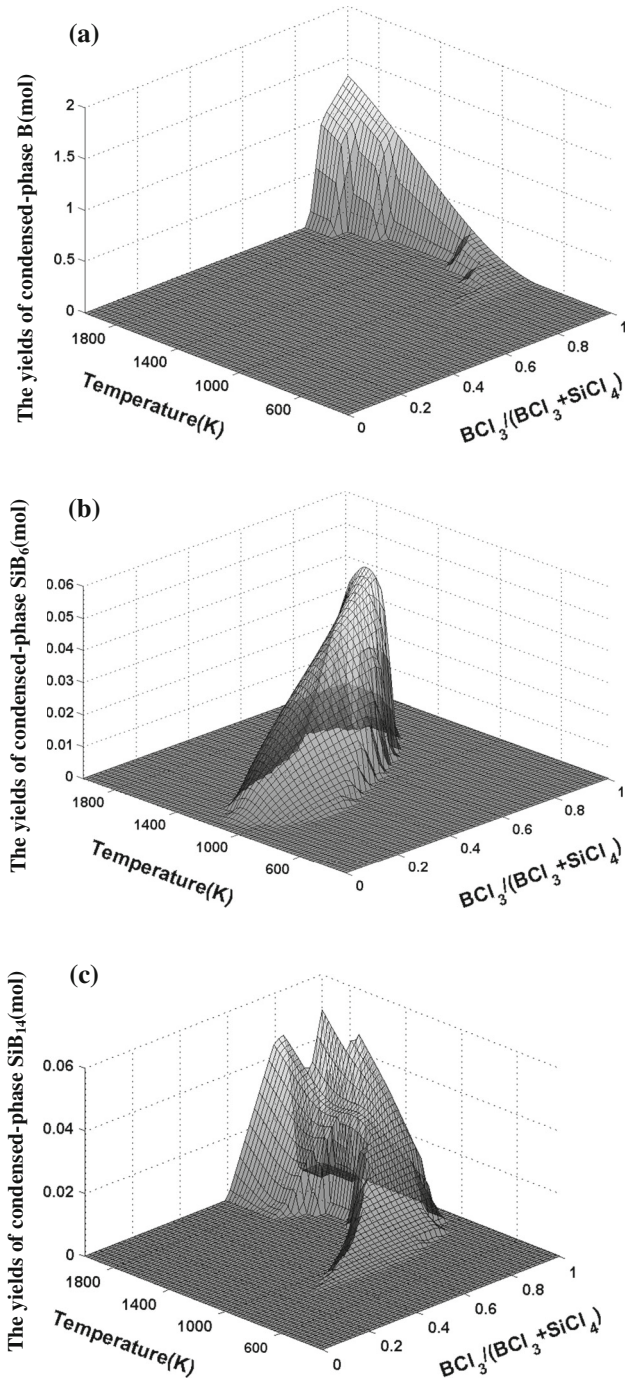

Fig. 4 Production of the condensed phases as a function of temperature and r ratios of $BCl_3/(BCl_3 + SiCl_4)$

Effects of temperature and ratios of $BCl_3/(BCl_3 + SiCl_4)$ on condensed phases

In all of the calculations, the total pressure is 1 atm, and the total amount of the reactants and diluents gases BCl_3, $SiCl_4$, H_2, and Ar are fixed at 5.0 mol. However, the moles of BCl_3 and $SiCl_4$ can be variant to yield an expected ratio of $r = BCl_3/(BCl_3 + SiCl_4)$.

Figure 4a–c shows, respectively, the production of the condensed phases B, SiB_6, and SiB_{14} at temperatures within 300–2,000 K and the ratios of $BCl_3/(BCl_3 + SiCl_4)$ within 0–1.0. It shows that both temperature and r ratio have significant influence on the production of the condensed phases. Figure 4a shows that only the r ratios above 0.8 can produce the condense phase B. Figure 4b shows that the amount of SiB_6 increases sharply with r in 0.1–0.8 and temperature in 700–1,550 K. Figure 4c shows that the formation of a larger amount of the condensed phase SiB_{14} should have a higher r ratio (>0.7) and a higher temperature (>1,400 K).

Conclusions

The equilibrium distribution of a relatively complete set of the 220 species (4 atoms and 211 polyatomics, 5 condensed phase species) that might be involved in the CVD preparation of the silicon borides in the BCl_3–$SiCl_4$–H_2 system was studied thermodynamically. The structures and the thermochemical data for 128 (among the 211) species were determined theoretically. The structures were optimized with DFT B3PW91/6-31G(d) method. The heat capacities and entropies were evaluated with the standard statistical thermodynamics by using the structures and vibrational frequencies obtained at B3PW91/6-31G(d) level. The electronic excitation energies from TD-DFT at B3PW91/6-31G(d) level were involved in the statistical thermodynamics treatments. Accurate model chemistry G3(MP2) and G3//B3LYP theories were employed to calculate the accurate molecular energies.

The equilibrium concentration distribution determined by using the fundamental data (developed in this work and in references) and by employing the chemical equilibrium principle in the BCl_3–$SiCl_4$–H_2 system shows that $SiCl_4$ and BCl_3 initially react at temperatures higher than 500 K, and the condensed boron appeared at temperatures in 800–900 K. $BHCl_2$, $SiHCl_3$, and BH_2Cl are found to be the crucial intermediates.

The production of the condensed phases strongly depends on the molar ratio of $r = BCl_3/(BCl_3 + SiCl_4)$ and quite sensitive to temperature. The ideal deposition ratio r for B should be above 0.8. The amount of SiB_6 increases sharply with r in 0.1–0.8 and temperatures in 700–1,550 K. Formation of a larger amount of the condensed phase SiB_{14} should have a higher r (>0.7) and a higher temperature (>1,400 K).

This work provides more fundamental data for analyzing the thermochemistry of the CVD process of the BCl_3–$SiCl_4$–H_2 system at any ratio of the input precursors to control the formation of the condensed phase B, SiB_6, and SiB_{14}.

Acknowledgments This work is supported by the Basic Research Foundation of NWPU (No. JCY20130114), the National Natural Science Foundation of China (Nos. 51372203, 51332004), Foreign Talents Introduction and Academic Exchange Program of China (No. B08040), and the fund of the State Key Laboratory of Solidification Processing in NWPU (No. SKLSP201317). The authors also acknowledge the High Performance Computing Center of NWPU for the allocation of computing time on their machines.

References

1. White SR, Sottos NR, Geubelle PH, Moore JS, Kessler MR, Sriram SR (2001) Autonomic healing of polymer composites. Nature 409:794–797
2. Quemard L, Rebillat F, Guette A, Tawil H, Louchet-Pouillerie C (2007) Self-healing mechanisms of a SiC fiber reinforced multilayered ceramic matrix composite in high pressure steam environments. J Eur Ceram Soc 27:2085–2094
3. Raman V, Bhatia G, Mishra A, Sengupta PR, Saha M (2005) Development of carbon–ceramic composites. Mater Sci Eng A 412:31–36
4. Schulte-Fischedick J, Schmidt J, Tamme R, Kroner U, Arnold J, Zeiffer B (2004) Oxidation behaviour of C/C–SiC coated with SiC–B_4C–SiC–cordierite oxidation protection system. Mater Sci Eng A 386:428–434
5. Cutard T, Huger M, Fargeot D, Gault C (1993) In: Naslain R (ed) Proc HT-CMC1. Abington Cambridge, Woodhead, pp 33–49
6. Lamouroux F, Camus GJ (1994) Oxidation effects on the mechanical properties of 2D woven C/SiC composites. J Eur Ceram Soc 14:177–188
7. Liu YS, Cheng LF, Zhang LT, Wu SJ, Yang WB (2007) Oxidation protection of multilayer CVD SiC/B/SiC coatings for 3D C/SiC composite. Mater Sci Eng A 466:172–177
8. Zhang LT, Cheng LF, Xu YD, Liu YS, Zeng QF, Dong N, Luan XG (2006) Progress on self-healing silicon carbide ceramic matrix composites and its applications. J Aeronaut Mater 3:226–232
9. Lamouroux F, Bertrand S, Pailler R (1999) Oxidation-resistant carbon-fiber-reinforced ceramic-matrix composites. Compos Sci Technol 59:1073–1085
10. Naslain R, Lamon J, Pailler R et al (1999) Micro/minicomposites: a useful approach to the design and development of non-oxide CMCs. Compos Part A 30:537–547
11. Yang WB, Zhang LT, Liu YS, Cheng LF, Zhang WH (2007) Preparation and mechanical properties of carbon fiber reinforced $(BC_x–SiC)_n$ multilayered matrix composites. Appl Compos Mater 14:277–286
12. Naslain R, Pailler R, Bourrat X et al (2001) Synthesis of highly tailored ceramic matrix composites by pressure-pulsed CVI. Solid State Ionics 141–142:541–548
13. Taguchi T, Nazawa T, Iagawa N (2004) Fabrication of advanced SiC fiber/F-CVI SiC matrix composites with SiC/C multi-layer interphase. J Nucl Mater 329–333:572–576
14. Maxwell JL, Chavez CA, Springer RW, Maskaly KR, Goodin D (2007) Preparation of superhard B_xC_y fibers by microvortex-flow hyperbaric laser chemical vapor deposition. Diam Relat Mater 16:1557–1564
15. Santos MJ, Silvestre AJ, Conde O (2002) Laser-assisted deposition of r-B_4C coatings using ethylene as carbon precursor. Surf Coat Technol 151–152:160–164
16. Peshev P (2000) A thermodynamic estimation of the chemical vapor deposition of some borides. J Solid State Chem 154:157–161
17. Sezgi NA, Dogu T, Ozbelge HO (1999) Mechanism of CVD of boron by hydrogen reduction of BCl3 in a dual impinging-jet reactor. Chem Eng Sci 54:3297–3304
18. Koh M, Nakajima T (1999) Electrochemical behaviors of carbon alloy BC_x and of BC_x-coated graphite prepared by chemical vapor deposition. Electrochim Acta 44:1713–1722
19. Shirai K, Emura S, Gonda S, Kumashiro Y (1995) Infrared study of amorphous $B_{1-x}C_x$ films. J Appl Phys 78:3393–3400
20. Jacobsohn LG, Nastasi M (2005) Sputter-deposited boron carbide films: structural and mechanical characterization. Surf Coat Technol 200:1472–1475
21. Berjonneau J, Langlais F, Chollon G (2007) Understanding the CVD process of (Si)–B–C ceramics through FTIR spectroscopy gas phase analysis. Surf Coat Technol 201:7273–7285
22. Shen P, Zou BL, Jin SB, Jiang QC (2007) Reaction mechanism in self-propagating high temperature synthesis of TiC–TiB_2/Al composites from an Al–Ti–B_4C system. Mater Sci Eng A 454–455:300–309
23. Allendorf MD, Melius CF (1998) Understanding gas-phase reactions in the thermal CVD of hard coatings using computational methods. Surf Coat Technol 108–109:191–199
24. Frisch MJ, Trucks GW, Schlegel HB, Scuseria GE, Robb MA, Cheeseman JR, Scalmani G, Barone V, Mennucci B, Petersson GA, Nakatsuji H, Caricato M, Li X, Hratchian HP, Izmaylov AF, Bloino J, Zheng G, Sonnenberg JL, Hada M, Ehara M, Toyota K, Fukuda R, Hasegawa J, Ishida M, Nakajima T, Honda Y, Kitao O, Nakai H, Vreven T, Montgomery JA Jr, Peralta JE, Ogliaro F, Bearpark M, Heyd JJ, Brothers E, Kudin KN, Staroverov VN, Kobayashi R, Normand J, Raghavachari K, Rendell A, Burant JC, Iyengar SS, Tomasi J, Cossi M, Rega N, Millam JM, Klene M, Knox JE, Cross JB, Bakken V, Adamo C, Jaramillo J, Gomperts R, Stratmann RE, Yazyev O, Austin AJ, Cammi R, Pomelli C, Ochterski JW, Martin RL, Morokuma K, Zakrzewski VG, Voth GA, Salvador P, Dannenberg JJ, Dapprich S, Daniels AD, Farkas O, Foresman JB, Ortiz JV, Cioslowski J, Fox DJ (2009) Gaussian 09, Revision A.02. Gaussian Inc., Wallingford
25. Su K, Wei J, Hu X, Yue H, Lu L, Wang Y, Wen Z (2000) Systematic comparison of geometry optimization on inorganic molecules. Acta Phys Chim Sin 16:643–651
26. Su K, Wei J, Hu X, Yue H, Lu L, Wang Y, Wen Z (2000) High-level ab initio energy divergences between theoretical optimized and experimental geometries. Acta Phys Chim Sin 16:718–723
27. Curtiss LA, Redfern PC, Raghavachar K, Rassolov V, Pople JA (1999) Gaussian-3 theory using reduced Møller–Plesset order. J Chem Phys 110:4703–4709
28. Baboul AG, Curtiss LA, Redfern PC, Raghacachari K (1999) Gaussian-3 theory using density functional geometries and zero-point energies. J Chem Phys 110:7650–7657
29. Deng JL, Su KH, Zeng Y et al (2008) Investigation of thermodynamic properties of gaseous SiC(X_{3P} and a_{1R}) with accurate model chemistry calculations. Phys A 387(22):5440–5456
30. Scott AP, Radom L (1996) Harmonic vibrational frequencies: an evaluation of Hartree–Fock, Møller–Plesset, quadratic configuration interaction, density functional theory, and semiempirical scale factors. J Phys Chem 100:16502–16513
31. Petersilka M, Gossmann UJ, Gross EKU (1996) Excitation energies from time-dependent density-functional theory. Phys Rev Lett 76:1212–1215
32. Bauernschmitt R, Ahlrichs R (1996) Treatment of electronic excitations within the adiabatic approximation of time dependent density functional theory. Chem Phys Lett 256:454–464
33. Stratmann RE, Scuseria GE (1998) An efficient implementation of time-dependent density-functional theory for the calculation of excitation energies of large molecules. J Chem Phys 109:8218–8224

34. Yang SY, Kan YH, Yang GC, Su ZM, Zhao L (2006) TD-DFT investigation on the low-lying excited states of spiro-bithiophene. Chem Phys Lett 429:180–184
35. Barone V, Cimino P, Crescenzi O, Pavone M (2007) Ab initio computation of spectroscopic parameters as a tool for the structural elucidation of organic systems. J Mol Struct-Theochem 811:323–335
36. Zeng QF (2004) Optimized designation of C/SiC composite materials, PhD thesis, Northwestern Polytechnical University
37. Zeng Y, Su KH, Deng JL, Wang T, Zeng QF, Cheng LF, Zhang LT (2008) Thermodynamic investigation of the gas-phase reactions in the chemical vapor deposition of boron carbide with BCl_3–CH_4–H_2 precursors. J Mol Struct-Theochem 861:103–116
38. Deng JL, Su KH, Wang X, Zeng QF, Cheng LF, Xu YD, Zhang LT (2009) Thermodynamics of the gas-phase reactions in the chemical vapor deposition of silicon-carbide with methyltrichlorosilane precursor. Theor Chem ACC 122:1–22
39. http://webbook.nist.gov/chemistry/
40. Chase MW Jr (1998) J Phys Chem Ref. Data, Monograph No. 9
41. Lide DR (Ed. in Chief) (1996–1997) CRC handbook of chemistry and physics, 77th edn. CRC Press, Boca Raton
42. FactSage 5.4.1 (2006) Montreal, Quebec